Flight power muscles have a coordinated, causal role in hawkmoth pitch turns

Leo Wood[1,2], Joy Putney[1,3], Simon Sponberg[1,2,3,*]

[1]Quantitative Biosciences Program, Georgia Institute of Technology, Atlanta, GA 30313, USA

[2]School of Physics, Georgia Institute of Technology, Atlanta, GA 30313, USA

[3]School of Biological Sciences, Georgia Institute of Technology, Atlanta, GA 30313, USA

[*]Author for correspondence: sponberg@gatech.edu

Summary Statement

We investigate how individual muscles contribute to flight by manipulating muscle timing in behaving hawkmoths. We find precise timing of single muscles does not produce precise turns, highlighting the importance of coordination across the entire motor program.

Abstract

Flying insects solve a daunting control problem of generating a patterned and precise motor program to stay airborne and generate agile maneuvers. In this motor program, each muscle encodes information about movement in precise spike timing down to the millisecond scale. Whereas individual muscles share information about movement, we do not know if they have separable effects on an animal's motion, or if muscles functionally interact such that the effects of any muscle's timing depend heavily on the state of the entire musculature. To answer these questions, we performed spike-resolution electromyography and electrical stimulation in the hawkmoth *Manduca sexta* during tethered flapping. We specifically explored how flight power muscles contribute to pitch control. Combining correlational study of visually-induced turns with causal manipulation of spike timing, we discovered likely coordination patterns for pitch turns, and investigated if these patterns can drive pitch control. We observed significant timing change of the main downstroke muscles, the dorsolongitudinal muscles (DLMs), associated with pitch turns. Causally inducing this timing change in the DLMs with electrical stimulation produced a consistent, mechanically relevant feature in pitch torque, establishing that power muscles in *Manduca* have a control role in pitch. Because changes were evoked in only the DLMs, however, these pitch torque features left large unexplained variation. We find this unexplained variation indicates significant functional overlap in pitch

Journal of Experimental Biology • Accepted manuscript

control such that precise timing of one power muscle does not produce a precise turn, demonstrating the importance of coordination across the entire motor program for flight.

KEYWORDS: Motor control, neuromechanics, *Manduca*, flight, pitch, stimulation

Introduction

Locomoting animals have to generate a motor program, a coordinated spatial and temporal pattern of activity sent to an array of muscles to produce behaviors. Each muscle is controlled by action potentials, or spikes, which carry information about the motion of an animal to a highly precise millisecond or sub-millisecond scale (Putney et al., 2019; Sober et al., 2018). This is significant because the degree to which muscles are *functionally* coordinated, such that the kinematic and behavioral action of individual muscles depends on the action of other muscles, determines how precise spike timing translates to movement. If a single muscle independently controls specific features of kinematics or dynamics, then precisely timed spikes to that muscle can be directly attributed to precise behavioral outcomes. But if control is orchestrated across many muscles simultaneously such that the action of one muscle changes the potential of another muscle to do control, then the transformation of a precise change in spike timing into movement will depend on the context created by the spiking patterns in the rest of the motor program. Such a dependency might be expected since muscles often act in coordinated groups (Ting, 2007), produce context-dependent mapping between bulk muscle activation and kinematics (Kutch and Valero-Cuevas, 2011; Valero-Cuevas, 2009) and can share information even at the level of individual spikes (Putney et al., 2019). But does this shared information translate into functional coordination, or do individual muscles have separable, independent effects on behavioral outcomes?

Insect flight provides a particularly tractable system for studying this question. While flight is a complex, 3-dimensional form of locomotion, in many orders of flying insects such as Diptera and Lepidoptera, as few as 12 muscles— all effectively single motor units (Rheuben, 1985; Usherwood, 1962)—generate all of the motion and control of the wings (Lindsay et al., 2017; Putney et al., 2019). This motor program is separated into indirect flight muscles and a set of steering muscles that directly attach to the wing, all contained within the thorax of the body. Two large pairs of flight power muscles, the dorsolongitudinal muscles (DLMs) and dorsoventral muscles (DVMs), produce most of the mechanical power for flight, while smaller steering muscles directly deform the wing hinge to adjust wing kinematics (Eaton et al., 1988). Steering muscles are well known to perform flight control, with timing of individual muscles often correlated to specific maneuvers and wing kinematics (Ando and Kanzaki, 2004; Balint and Dickinson, 2004; Dickinson and Tu, 1997; Hedenström, 2014; Lindsay et al., 2017; Melis et al., 2024; Sadaf et al., 2015; Tu and Dickinson, 1996; Wang et al., 2008; Whitehead et al., 2022). However in larger synchronous insects such as the hawkmoth *Manduca sexta*, the timescale of power muscle force production is well within a single wingstroke (Tu and Daniel, 2004), providing a clear case where both

power and steering muscles are actively involved in flight control (Ando and Kanzaki, 2016; Sponberg and Daniel, 2012; Sponberg et al., 2015a). Hawkmoths generally provide an excellent window into muscle coordination, especially through the lens of spike timing, as a comprehensive flight motor program can be recorded to a spike-level resolution in a behaving animal, simultaneous with time-resolved body forces and torques (Putney et al., 2019).

In hawkmoths, then, is the motor program functionally coordinated? The hawkmoth flight motor program is known to be sub-millisecond precise (Putney et al., 2019; 2023b), and correlational evidence suggests a high degree of coordination and overlapping control potentials. In an information-theoretic sense, the hawkmoth flight motor program is coordinated so that spike timing of all muscles carries redundant global information about behavioral output (Putney et al., 2019). Linear combinations of muscle activity also explain the behavioral output of multiple different turning maneuvers, allowing 90% accurate decoding of the type of turn maneuver performed from activity of only 4 or more muscles (Putney et al., 2021). In some functionally coordinated systems, linear combinations of commands across multiple muscles called muscle synergies can describe the majority (often >90%) of output variation (Ting, 2007). However, yaw turning behaviors in hawkmoths were better described by the independent activity of muscles than as a synergy (Sponberg et al., 2015a). These lines of evidence are mixed, suggesting that muscles in the hawkmoth flight motor program have overlapping control potentials, but do have potentially independent effects on an animal's motion.

A major driver of this conflicting picture is that when the spike timing of *many* muscles may be correlated with behavior, it is challenging to separate the causal contributions of individual muscles to a given behavioral output. Direct electrical stimulation of muscles and motor neurons can reveal a muscle's control potential, by causally inducing specific spike timing in specific situations. As an *in vivo* manipulation of muscle activity, electrical stimulation has been used to identify muscle control potentials in anesthetized vertebrates (Vazquez, 1995), elicit control changes in flying insects via high frequency stimulation (Sato and Maharbiz, 2010; Sato et al., 2015), or perform bulk perturbation to specific sides of an insect (Tsang et al., 2010). More rarely, however, it can be applied in behaving invertebrates to produce targeted, spike-level manipulations of specific muscle timings (Sponberg et al., 2011). In hawkmoths, altering motoneuron spike timing shows a causal connection between left-right timing differences in primary downstroke muscles and yaw torque (Sponberg and Daniel, 2012). However, for flying insects these temporally precise manipulations and related correlational studies have only focused on left-right asymmetries leading to roll or yaw turns (Fernández et al., 2012; Sponberg and Daniel, 2012; Sponberg et al., 2015a; Springthorpe et al., 2012; Wang et al., 2008). Causal manipulation of steering muscles to produce pitch turns has been performed in fruit flies using optogenetics (Whitehead et al., 2022), but for flying insects no spike-level manipulations have been performed to study pitch turns.

Gaps such as these are notable because pitch turns are particularly interesting for hovering insects. Nearly every model of insect flight dynamics identifies an unstable mode resulting from coupled oscillations in fore-aft velocity and pitch, requiring some degree of active neuromuscular control (Kim and

Han, 2014; Kim et al., 2015; Ristroph et al., 2013; Windsor et al., 2014). Active control of pitch must also be bilaterally symmetric by nature, so any control cannot simply result from left-right motor program asymmetries (Jankauski et al., 2017). Though flying insects such as dipterans and lepidopterans control pitch through a multifaceted set of passive and active mechanisms, including passive vibrational stability via wing oscillation (Taha et al., 2020) and movement of the center of mass (COM) relative to the center of pressure (COP) via abdominal motion (Frye, 2001; Hedrick and Daniel, 2006; Hinterwirth and Daniel, 2010; Le et al., 2023; Ristroph et al., 2013), most pitch control is thought to arise from the activity of the steering muscles (Whitehead et al., 2015; 2022). While modulation of spike timing in the flight power muscles has been closely linked to roll and yaw turns (Lehmann et al., 2013; Sponberg and Daniel, 2012; Sponberg et al., 2015a; Springthorpe et al., 2012), it is not known to what degree power muscles can also control pitch turns. Such turns require not left-right phase separation but modulation of kinematics between the downstroke and upstroke. If the indirect power muscles are capable of contributing to pitch control, they must do so through alteration of wing kinematics, either moving the COP, changing time-varying wing forces, or producing inertial moments on the COM. In freely flying hawkmoths pitching up in response to looming stimuli correlates with changes in angle of attack, stroke plane tilt, angle at wingstroke reversals, and deviation angle at wingstroke reversals (Cheng et al., 2011). The interval between the DLM and DVM has been implicated in changing deviation angle of the wing in free flight (Wang et al., 2008), and shown to change with flight speed in forward flight, so may be related to modulating power production (Hedrick et al., 2017).

Overall, however, while the precise spike timing of the hawkmoth power muscles has been connected to asymmetric kinematics, their potential for control on other maneuvers such as pitch turns are unclear. We hypothesize that the indirect power musculature in the hawkmoth *Manduca sexta* does contribute to pitch control. We also hypothesize that the flight motor program is functionally coordinated, such that even the mapping of individual action potentials of large power muscles into movement (the muscle's control potential) (Sponberg et al., 2011) is dependent on the context of the rest of the motor program. Alternatively, we might see that the flight motor program is not very functionally coordinated, so that the control potentials of individual muscles are easily identified and not affected by the activity of other muscles. Using a combination of correlational and causal experiments, we test both of these hypotheses, identifying an association between power muscle activity and pitch turns, then rewriting motor activity to reproduce those patterns in tethered flight.

Materials and Methods

Animals

All moths (*M. sexta*) were obtained as pupae and housed communally after eclosion with a 12 hour light-dark cycle (N = 9, University of Washington colony and Carolina Biological Supply Co for visually-induced turning experiments; N = 5, Case Western Reserve colony for stimulation experiments). Naive males and

females were used in experiments conducted during the dark period of their cycle. EMG recordings were performed on cold-anesthetized moths by inserting pairs of silver wire (diameter 0.005*in*) into the thorax and fastening them with cyanoacrylate glue, following the same procedure as (Putney et al., 2019). After wire insertion, moths were fastened with cyanoacrylate to a tether rigidly attached to a custom six-axis load cell (ATI Nano17ti, FT20157; calibrated ranges $F_x, F_y = \pm 1.0\ N$, $F_z = \pm 1.8\ N$, $\tau_x, \tau_y, \tau_z = \pm 6.25\ mNm$). After attachment moths were left to dark adapt for 30 minutes at luminance levels typical for when these crepuscular moths are active (Sponberg et al., 2015b).

High-amplitude optomotor turns in visual arena experiments

The data of constant high amplitude optomotor-induced turns were originally published by Putney et al (Putney et al., 2021). Moths were presented with wide-field sinusoidal gratings on a rendered 3D sphere in Microsoft Visual Studio (Fig. 1). The stimuli were projected onto three computer monitors (ASUS PG279Q ROG Swift; 2560 x 1440 px) overlaid with neutral density filters to obtain peak sensitivity luminance conditions for *Manduca* of approximately 1 $cd\ m^{-2}$ (Stöckl et al., 2017). The tethering set-up placed the moth at the center of a three-sided box formed by these three monitors (Fig. 1A). The sinusoidal gratings had a spatial frequency of 20 $^\circ\ cycle^{-1}$, and the sphere was rotated to place its axis of rotation along each of the earth-coordinate system flight axes of pitch, roll, and yaw (Fig. 1B). The sphere was then rotated about this axis in opposite directions at a constant drift velocity of 100 $^\circ\ s^{-1}$ (5 $cycle\ s^{-1}$), which was chosen since this spatiotemporal frequency drove high responses in the moth visual system (Stöckl et al., 2017). Therefore, each moth responded to six distinct visual stimulus conditions, three pairs about each flight axis: pitch up (PU), pitch down (PD), roll left (RL), roll right (RR), yaw left (YL), and yaw right (YR).

Simultaneous strain gauge voltage recordings from the F/T transducer and EMG recordings from the silver wire electrodes were taken as the moth responded to each of the six stimulus conditions for 20 seconds, each recorded at 10 kHz. The strain gauge voltages were converted to the three forces and three torques on each axis at the estimated average COM for tethered moths. These forces and torques were lowpass filtered using a 8th order Butterworth filter with a cutoff of 1000 Hz. To segment wing strokes in some analyses, a type II Chebyshev filter was applied to F_z with a bandpass between 5 and 35 Hz to capture the range of wingbeat frequencies observed in this dataset (15 - 27 Hz). The Hilbert transform of this filtered signal was taken to estimate the wingstroke phase, and individual wingstrokes were separated by finding negative-to-positive zero crossings of this phase, with $t = 0$ for each wingstroke occurring at these crossings. This use of the Hilbert transform to find instantaneous phase and separate a gait into specific cycles has previously been used in hawkmoths (Putney et al., 2019; Sponberg et al., 2015a), gait analysis of cockroaches (Revzen and Guckenheimer, 2008), and rat whisking (Hill et al., 2011). Spikes in the raw EMG voltage recordings were discriminated using Offline Sorter (OFS; Plexon) via threshold crossing. Where necessary, filtering options in this software were used

to correct baseline wander, motion artifacts, and other noise that made discriminating spikes difficult. Spike times were specified to 0.1 ms relative to zero phase in each wing stroke as described above.

Centered wingstroke mean torques were used to compare between opposing conditions in pitch, roll, and yaw (Fig. 1E). Centering was performed by subtracting from per-wingstroke mean pitch, roll, and yaw torques the per-moth overall mean pitch, roll, and yaw torques τ_x, τ_y, τ_z across all that moth's data for both conditions (i.e. both pitch up and pitch down turns). Centering was performed independently for each moth ($N = 9$ moths).

Electrical stimulation experiments

To causally manipulate power muscle timing and observe resulting changes in flight forces and torques, electrical stimulation was used to alter the spike timing of the dorsolongitudinal muscles (DLMs). While there are many previous studies eliciting control changes in flying insects using high frequency electrical stimulation (Sato and Maharbiz, 2010; Sato et al., 2015) or bulk stimulation of individual sides of an insect (Tsang et al., 2010), here we use targeted and precisely timed stimulation to induce single action potentials in the DLMs, in a method more akin to (Sponberg and Daniel, 2012; Sponberg et al., 2011).

Moths attached to a 6-axis load cell tether would freely engage in bouts of flapping flight, during which the DLMs would be stimulated with a specific timing relative to the DVMs. Stimulus delay times were chosen at random from a range of 4-40 ms after DVM spike detection, with each delay time applied for a 20 second recording period with EMG and F/T transducer recorded at 10 kHz. Single 0.25 ms pulses of either constant current or constant voltage were applied to silver wires placed on either end of each DLM, with each stimulation separated by at least 4 seconds to avoid entrainment. A diagram signal flow used for stimulation is shown in Fig. 2A. In brief, timing of stimulus was achieved by passing either the left or right DVM voltage recording through a custom analog spike-detection circuit and microcontroller. The controller would trigger a stimulator (A-M Systems Model 3800) with a stimulus isolation unit (A-M Systems Model 2200) on a controlled delay time from the onset of a detected DVM spike.

All stimulus pulses were biphasic, but specific stimulus features were calibrated for each moth individually, such as whether constant current or voltage were used and of what amplitude. This calibration in an example moth is shown in Fig. 2B. Stimulus was repeatedly applied while the moth was in a quiescent state, with stimulation amplitude steadily increased until evoked motor action potentials were observed in both DLMs with no evoked action potentials observed in surrounding muscles (Fig. 2B). While most individuals had their best response from constant current stimulation, differences in electrode placement and individual anatomy and physiology resulted in better results for some individuals from constant voltage stimulation. After calibration, stimuli ranged from 0.05-0.1 mA for constant current stimulation and 5-10 V for constant voltage. Note that, as shown in Fig. 2B, evoked action potentials occur roughly 4 milliseconds after a pulse of current is applied.

Spike discrimination, wingstroke segmentation, and FT data calibration and filtering followed the same parameters as described previously (Putney et al., 2019), with several exceptions. As the load cell the moth is tethered to measures forces and torques at a distance from the moth's actual COM (which is typically between the thorax and the first abdominal segment), strain gauge voltages had to be transformed to COM locations estimated for each individual. This estimation was performed using bounded linear least-squares minimization to find the COM location which minimized torques to zero during fully quiescent data of each tethered moth. Different filter parameters were used for wingstroke segmentation, specifically a 4^{th} order type II Chebyshev filter with a 10-40 Hz passband, as this demonstrated better wingstroke segmentation performance for the stimulation data.

Stimulation trials were included in this study only if stimulus evoked a muscle action potential (MAP) in both DLMs, and if the first observed MAP from both DLMs in the stimulus wingstroke was evoked rather than natural. MAPs were deemed evoked rather than natural if they occurred within a 5ms window directly following stimulation. Figure 2D provides a visual aide for how evoked MAPs were selected; wingstrokes were only included if both left and right DLMs had a MAP occur along the main diagonal of Fig. 2D, and if the first spike in the stimulation wingstroke occurred along this diagonal.

Feature extraction and stimulation analysis

To analyze the effects of controlled DLM timing on pitch torque, features of pitch torque which were associated with evoked DLM timing had to be extracted and quantified. To extract features of pitch torque that correlated with stimulation-evoked changes in DLM timing, canonical correlation analysis (CCA) was employed with the cross decomposition module of the *scikit-learn* python package (Pedregosa et al., 2011), which utilizes a previously described algorithm (Wegelin, 2000). CCA is one of several dual-dimensionality reduction methods, such as partial least squares regression (PLS) (Sponberg et al., 2015a; Wegelin, 2000), where two sets of latent variables (or "features") $\boldsymbol{T}'$ and $\boldsymbol{Y}'$ which maximally correlate with each other are extracted from two sets of original data variables $\boldsymbol{T}$ and $\boldsymbol{Y}$. CCA is very closely related to the commonly used principal components analysis (PCA) in that it uses an eigendecomposition to construct components (or "features") from a linear combination of variables in a dataset. In PCA, these features are constructed to maximize variance, whereas in CCA and the broader family of PLS, two sets of features which maximally correlate with each other are constructed simultaneously from two sets of variables. By inputting the set of pitch torque waveforms for $\boldsymbol{T}$ and the stimulation-evoked DLM timing or phase for $\boldsymbol{T}$, we can extract a feature of the pitch torque data, $\boldsymbol{T}'$, which maximally correlates with evoked timing changes.

CCA was performed on each individual moth independently with pitch torque data assembled into a matrix $\boldsymbol{T}$ and stimulation-evoked DLM phase assembled into a matrix $\boldsymbol{Y}$. Pitch torques for all stimulation wingstrokes were linearly interpolated to $m = 300$ samples long and assembled into an $n \times m$ matrix $\boldsymbol{T}$, where n is the number of valid stimulation wingstrokes for that individual. The other CCA input, $\boldsymbol{Y}$, was

constructed as an $n \times k$ matrix of just a single variable, the phase of the evoked DLM spike for each stimulation wingstroke ($k = 1$ for the duration of this paper).

Note that CCA was performed on z-scored versions of $\boldsymbol{T}$ and $\boldsymbol{Y}$, denoted throughout by caret hats as $\widehat{\boldsymbol{T}}$ and $\widehat{\boldsymbol{Y}}$, respectively. Z-scoring allows for more stable operation on data of different ranges and units by making variance nondimensional and placing disparate data in similar ranges. Note that when quantities are provided in real units z-scoring is inverted.

For $\boldsymbol{T}$ and $\boldsymbol{Y}$, CCA produces a $k \times m$ set of features often referred to as "loadings" $\boldsymbol{T}_{loadings}$, an $m \times k$ set of "weights" used to construct the features $\boldsymbol{T}_{weights}$, and an $n \times k$ set of "scores" defined by $\boldsymbol{T}\boldsymbol{T}_{weights}$, effectively the projection of the data in $\boldsymbol{T}$ to the reduced set of features $\boldsymbol{T}'$. Data in $\boldsymbol{T}$ can be reconstructed from the features in $\boldsymbol{T}_{loadings}$

$$\hat{R} = \mathbf{T}_{\text{scores}}\boldsymbol{T}_{loadings}^{T} \tag{1}$$

where $\hat{R}$ is an $n \times m$ matrix of approximations of the original data in $\boldsymbol{T}$ via linear scaling of the feature vector $\boldsymbol{T}_{loadings}$. Note that, denoted by the caret hat, $\hat{R}$ is still z-scored, and the inverse of the z-scoring is applied to obtain values with real units.

Angular impulse, or net change in angular momentum, was calculated from pitch torque of extracted features and original pitch torque data for individual wingstrokes as

$$\Delta L = \int_{t_1}^{t_0} \tau_x dt \tag{2}$$

where t_0 and t_1 define the start and end times of the wingstroke, respectively. We obtain effective pitch angular velocity due to pitch torque as

$$\Delta\omega = \frac{\Delta \mathrm{L}}{I_{yy}} \tag{3}$$

where I_{yy} is the pitch moment of inertia for *Manduca sexta*, defined throughout this work as $I_{yy} = 266.7\ gmm^2$ from (Cheng et al., 2011). Numerical integration was performed with the trapezoidal method, with CCA feature reconstructions resampled from $m = 300$ to the original number of samples present in the corresponding wingstroke.

Any testing for significant linear relationships between induced DLM timing and aggregate variables of flight mechanics, such as pitch angular impulse or wingstroke-averaged forces and torques, were performed using a linear mixed effects model in R (R Core Team, 2020) using the *nlme* library (Pinheiro et al., 2020). All models were fit with individual moth as a random intercept effect, with effect significance determined by a $p < 0.05$ cutoff.

Results

We investigated the relationship between precise spike timing of the flight power muscles in *Manduca sexta* and pitch turns through two main approaches. In the first experiment, $n = 21{,}203$ total wingstrokes were analysed from $N = 9$ moths induced to perform roll, pitch, and yaw turns through rotating wide-field visual stimuli to correlate how timing of the primary flight muscles changed between pitch up and pitch down turns. In the second experiment, in $n = 345$ wingstrokes across $N = 5$ moths we causally manipulated the timing of the primary downstroke muscles, the DLMs, to observe changes in pitch torque due to altering the relative timing of the primary flight power muscles.

Power muscle spike timing correlates with pitch turns in visually-induced turns

Mean centered torques for each condition showed separation on the expected axis (Fig. 1E), demonstrating that each condition indeed elicited a strong turn response from moths in only the desired direction. For instance, overall mean wingstroke torques per individual moths ($N = 9$) were statistically significantly different between mean pitch torque τ_x ($p = 0.003$ in paired t-test), but not between mean roll or yaw torques ($p > 0.05$ in paired t-tests for τ_y and τ_z).

When moths responded to pitch conditions, the time between the DLM spike and the first DVM spike increased in duration when pitching up (Fig. 3). In absolute time, mean duration between spikes across same-side DLM-DVM pairs was significantly different between pitch up and pitch down conditions (pitch up 24.5 ± 0.8ms, pitch down 17.6 ± 0.7 ms) (Fig. 3A-B,E). Interestingly, wingbeat frequency was much lower in pitch up than pitch down conditions in all moths, with mean wingbeat frequency of 18.6 ± 0.4 Hz in pitch up and 22.9 ± 0.5 Hz in pitch down (Fig. 3F). This could indicate that moths lower their wingbeat frequency when executing pitch up maneuvers. Because there is a change in wingbeat period between pitch up and pitch down conditions of ≈10.1 ms which could account for the observed difference in $t_{DVM} - t_{DLM}$ in absolute time, we normalized $t_{DVM} - t_{DLM}$ to the length of each wingstroke (Fig. 3C-D,G). Mean phase between same-side DLM-DVM pairs was $45 \pm 1\%$ of the wingstroke in pitch up conditions and $40 \pm 1\%$ in pitch down conditions, with the majority of individuals showing this trend (Fig. 3G).

Together these results demonstrate a correlation between DLM and DVM timing and pitch turns: In pitch up, the time between DLM and DVM spikes is greater, and in pitch down the time is reduced. While these data do not implicate any specific mechanisms or causal links between this timing shift and pitch turning, the high consistency of the observed timing shift suggests a functional role played by the power muscles in controlling pitch turns.

Altered DLM timing produces consistent changes to within-wingstroke pitch torque dynamics

Tuned, brief electrical stimulation can elicit MAPs in both of the main downstroke muscles of *Manduca sexta* without cross-stimulation of other muscles (Fig. 2B), including in tethered flapping when all flight muscles are highly active (Fig. 2C-D). Beyond simply inducing spikes, this method of electrical stimulation can perform a “motor overwrite”, fully preventing natural spikes from occurring in their normal timing, if the natural spikes are suppressed by the refractory period of the motor unit (Sponberg and Daniel, 2012). This is seen both in the provided example trace where only single spikes shifted earlier than their natural timing are observed in the stimulation wingstroke for both DLMs (Fig. 2C) and more generally in the complete data of spike times where stimulation applied in the 0.2-0.4 phase range visibly offsets or eliminates other spikes in the stimulation wingstroke (Fig. 2D). Causally manipulating DLM timing in single wingstrokes produced consistent and observable effects on within-wingstroke pitch torque (Fig. 4). When pitch torque traces are binned into groups by stimulation phase, pitch torque deviates from pre-stimulus wingstrokes (Fig. 4A-B). Typical wingstrokes have a 3- or 4-cycle oscillation in pitch torque which matches robotic flapping models of *Manduca* (Cheng et al., 2011), but evoked DLM spikes shifted the phase of these torque oscillations. Note that for all individuals, immediately after stimulation pitch torque initially pushes positive (head tilting downwards, as defined in Fig. 1A).

Stimulated wingstrokes show peak changes of 4 mNm or more compared to the immediately preceding wingstroke (Fig. 4). These changes lessen over the course of the wingstroke. Changes in torque were notably larger when the DLM was activated in early-wingstroke phases of less than 0.25. As a built-in control for the realism of evoked MAPs, for all individuals these changes due to stimulation progressively lessened as evoked DLM timing approached naturalistic timing around 40-50% of wingstroke phase.

In summary, changing the relative timing between the activation of downstroke and upstroke flight power muscles affects both mean pitch torque (Fig. 4C) and the deviation of mean pitch torque from normal dynamics (Fig. 4D). Altered DLM timing demonstrated consistent changes to within-wingstroke pitch torque dynamics in the form of a large oscillation in pitch torque following DLM spike phase, with the amplitude of this oscillation increasing the farther the DLM was evoked to spike relative to naturalistic timing. These features of causal manipulation of DLM timing, however, are purely qualitative. Surrounded by natural variation in pitch torque and the underlying motor program, features of pitch torque directly tied to evoked DLM timing are difficult to quantify without some form of directed feature extraction.

CCA features demonstrate power muscles have mechanically relevant influence on pitch torque

To determine whether the power muscles have a controllable influence on pitch, and how much variation in pitch torque is causally attributable to power muscle timing, requires quantifying the specific features of pitch torque associated with DLM phase. CCA was applied to extract these features of pitch torque which maximally covaried with evoked changes in DLM phase (Fig. 5). CCA features pick out the same observed trend in Fig. 4, with the main cyclic oscillations of pitch torque shifting earlier in phase as the DLM was induced to spike earlier. Notably, even a nonlinear kernel CCA extracts similar features (supplement Fig. S1) with only slightly higher variance explained, indicating that the underlying relationship between induced DLM phase and pitch torque is robust and well approximated by linear CCA.

If DLM phase has a causal, controllable effect on body pitch, the angular impulse (change in angular momentum) in the stimulation wingstroke should vary significantly with DLM phase. The angular impulse in pitch imparted by reconstructed CCA features (Eq. (2)) varied linearly with DLM phase (Fig. 6A) with a statistically significant positive slope across individuals ($p < 10^{-3}$). A significant slope is unsurprising, as CCA inherently finds features which maximally correlate with evoked DLM timing. CCA, however, is agnostic to the directionality of this relationship, so a positive slope indicates the maximally correlated relationship between these two variables is positive. Such a positive relationship indicates more negative angular momentum (more nose-up pitch) is linearly associated with a greater interval between the DLM and DVM, matching observations of the correlational experiment where greater $t_{DVM} - t_{DLM}$ was associated with pitching up (Fig. 3E).

To assess the behavioral relevance of these pitch torques, we divide angular impulse by pitch moment of inertia I_{yy}, giving the effective change in pitch angular velocity $\Delta\omega$ over a wingstroke (Eq. (3)). Change in pitch angular velocity over a wingstroke due to reconstructed features increased by at least 400 ° s^{-1} between early and late DLM phase in every individual (Fig. 6B). For a typical 50 millisecond wingstroke, 400 ° s^{-1} corresponds to a change of at least 20 ° in body pitch angle over a single wingstroke, a relevant amount of change from a flight control perspective. Pitch angular velocity of 400 ° s^{-1} is also well in line with free-flight pitching maneuvers pitch angular velocities observed to vary between -500 to +500 ° s^{-1} in *Manduca* (Cheng et al., 2011).

While it is clear that the features of pitch torque driven by the DLM demonstrate a causal and mechanically relevant influence on body pitch, there is a notable amount of unexplained variance of pitch torque in the stimulation wingstroke (Fig. 5D). On average across individuals, $64.5 \pm 6.7\%$ of the variance of pitch torque is not explained by a linear feature of evoked DLM phase. Similarly, the magnitude of pitch angular impulse due to CCA features is far smaller than overall pitch angular impulse (Fig. 6A). Though the angular impulse of CCA features alone had a statistically significant linear relationship with induced DLM timing, no such relationship is detectable between induced DLM timing and total angular impulse,

nor between induced DLM phase and any wingstroke-averaged torques (Fig. S3). Altogether this indicates that the degree to which muscles other than the DLM influence pitch torque is high, and the DLM does not control pitch in isolation.

Discussion

Power muscles contribute to pitch control in hawkmoth flight

The two experiments of this paper present correlational and causal evidence which supports the hypothesis that bilaterally symmetric changes in DLM spike timing alter body pitch. Greater time between the DLMs and DVMs leads to upwards pitch, and less time leads to downwards pitch. In the first experiment, pitch turns were visually induced and verified to produce separated responses in mean-centered torques only about the pitch axis (Fig. 1), and decreases in the phase between the DLM and DVM were observed in pitch down turns compared to pitch up (Fig. 3). This correlational finding was corroborated through causal manipulation of DLM-DVM timing (Fig. 2), where features of pitch torque that covaried with evoked DLM timing shifted towards downwards mean pitch as the time between the DLM and DVM decreased (Fig. 5). Bilaterallly asymmetric power muscle timing has been linked to control of yaw turns in flies and hawkmoths (Lehmann et al., 2013; Sponberg and Daniel, 2012; Tu and Daniel, 2004), and while in flies DLM motor neuron firing rate can modulate symmetric power and wingstroke amplitude (Gordon and Dickinson, 2006), to date no studies have shown symmetric power muscle timing causally affecting pitch. This is a particularly relevant finding, then, as pitch is part of an inherently unstable dynamic mode, and requires active control on relatively short timescales on the order of ≈ 45 *ms* for *Manduca* (Ristroph et al., 2013), similar to the duration of a typical wingbeat of ≈ 50 *ms*.

The ability for the indirect flight muscles to control pitch does not preclude known contributions from direct steering muscles in species including *Drosophila* (Whitehead et al., 2015; 2022) and *Manduca* (Ando and Kanzaki, 2004). This is consistent with induced changes in DLM timing relative to DVMs producing consistent pitch torque features, but the variance explained by these features being relatively low (Fig. 5D) and the angular impulse of these features, while relevant, presenting as small compared to overall impulse (Fig. 6).

A smaller influence of the indirect power muscles on pitch, however, is still behaviorally relevant. Despite often being much smaller than total pitch impulse, impulse from CCA features was large enough in all individuals to cause 400 $^\circ s^{-1}$ or more change in pitch angular velocity over single wingstrokes (Fig. 6). Both the amount of pitch imparted by CCA features and the ranges of DLM timing required to do so are highly plausible in free flight. The observed 400 $^\circ s^{-1}$ pitch velocity change closely matches the ±500 $^\circ s^{-1}$ pitch velocity observed in *Manduca* free flight (Cheng et al., 2011), and in natural, unmanipulated wingstrokes the DLM spikes between 20% to 55% of the wingstroke phase (Putney et al., 2019). So even

though the most pronounced effects of causally manipulating DLM phase on pitch torque occurred in earlier phases near 20-30% (Fig. 4D), these phases are consistent with the natural timing range of the DLM. Thus, while the overall effects of the DLM may only explain ≈ 40% of the variation in pitch torque, this is a relevant amount of variation when it comes to controlling the unstable mode of pitch as the observed effects on pitch from the DLM are reasonably expected to occur in natural free flight.

Possible mechanisms for power muscles to modulate pitch

For a flapping wing animal such as an insect, there are four possible ways to produce and modulate body pitch torque: 1) Move the location of the body center of mass (COM) relative to the wing center of pressure (COP) to change the moment arm on which aerodynamic forces are applied (e.g. abdominal flexion). 2) Modify the wingstroke-averaged or time-varying location of the COP in relation to the COM by altering wing kinematics (e.g. changing wing sweep angle). 3) Alter wing kinematics to generate inertial moments on the COM. 4) Change the within-wingstroke aerodynamic forces produced by the wings (e.g. changing the duration of the downstroke and upstroke to exploit moment asymmetries between the two phases of the wingstroke). Note that these mechanisms all interact and are not independent; varying wing kinematics will always change both aerodynamic and inertial forces. This means that of these four mechanisms, only the first (moving the COM relative to the COP) is unavailable to the indirect power muscles, as they are only able to alter wing kinematics.

Narrowing these four possible mechanisms down further, producing purely inertial moments is an unlikely mechanism to be used in isolation. For indirect power muscles, then, the most plausible kinematic mechanisms to exert pitch control are either by changing time-varying wing forces or moving the COP, both of which have been observed in hawkmoths. In freely flying hawkmoths wing pitch angle, or the spatial average rotation of the wing about its base-totip axis, correlates directly with body pitching movements (Cheng et al., 2011). As confirmed by a model robotic flapping wing, varying wing pitch angle had a clear effect of altering time-varying wing forces by altering the wing angle of attack. Increase the wingstroke mean wing pitch angle, and the angle of attack is increased during downstroke and decreased during upstroke, leading to a net nose-up pitching moment (Cheng et al., 2011). While the power muscles of hummingbirds do generate a wing pitch torque (Agrawal et al., 2022), it is unclear how hawkmoth power muscles could alter wing pitch angle, as the indirect hawkmoth power muscles have potentially less diverse effects on the wing's motion, primarily acting only on the stroke plane (Kammer, 1985). Instead in hawkmoths pitch angle is a kinematic quantity thought to be primarily controlled by direct steering muscles such as the 3rd axillary muscle (Ando and Kanzaki, 2004; Rheuben and Kammer, 1987).

Moving the COP relative to the COM is a more likely method for indirect power muscles to modulate pitch. Tilting of the wingstroke plane, while a well established option for controlling pitch (Taylor and Thomas, 2002; Willmott and Ellington, 1997; Zanker, 1988), is less plausible for power muscles which produce motion along the major stroke plane, and for which there is little evidence of a mechanism for

them to alter the angle of this plane. But altering the wing sweep, or angle the wings trace along the wingstroke plane, is a very plausible mechanism for power muscles to alter body pitch. Free flying hawkmoths are already known to asymmetrically reduce the ventral sweep amplitude to produce pitching moments (Willmott and Ellington, 1997). The timing of the DLM and DVM alter the wingstroke amplitude and sweep angle along the stroke plane from wingstroke to wingstroke in hawkmoths (Ando and Kanzaki, 2016; Wang et al., 2008). Adjusting the wingstroke sweep angle would change the COP location relative to the COM, allowing power muscles to control both pitch torques. Dipterans have long been known to use this mechanism of changing stroke amplitude to drive pitch control by shifting the wingstroke mean aerodynamic forces at the COP (Dickinson, 1999; Hollick, 1940; Nalbach and Hengstenberg, 1994; Taylor, 2001; Whitehead et al., 2015; 2022). For these reasons, of the possible kinematics mechanisms listed we find it most likely that power muscles in *Manduca* exert pitch control authority through wingstroke amplitude and sweep angle.

It is important to note that all data in this study comes from dorsally tethered moths. Tethering decreases wingstroke frequency of hawkmoths (Ando and Kanzaki, 2004), and is known to have an impact on kinematics (Fry et al., 2005), particularly on wing sweep and wingstroke amplitude. It is possible that the exact nature and amount of effect observed in pitch torque from altering DLM phase might differ in free flight. However, the repeatability of the DLM's effect on pitch torque across individuals and tendency of individual moths to have very different wing kinematics suggests the relationship between DLM phase and pitch torque is robust to the unperturbed state of wing kinematics.

That being said, it is clear the DLM does not act alone in controlling pitch, and that any pitch control potential from power muscles happens in concert with the control potential of direct steering muscles. The kinematic mechanisms we implicate for indirect power muscle control of wing sweep and wingstroke amplitude are already well known to be affected by steering muscles. In flies the 1st and 2nd basalar muscles contribute to the control of wing sweep and wingstroke amplitude on short timescales (Balint and Dickinson, 2001; Heide and Götz, 1996; Lehmann and Götz, 1996; Lindsay et al., 2017; Tu and Dickinson, 1996; Whitehead et al., 2015; 2022). Especially for synchronous flying insects such as hawkmoths, the direct flight musculature is always active (Kammer, 1971; Putney et al., 2019) and has an undeniable, constant role in any flight control. Our results demonstrate that the indirect power muscles have some control potential on body pitch, but this control potential can only occur in the context of the rest of the motor program and flight musculature.

Precisely changing the timing of one power muscle doesn't precisely determine a turn

Of important note is the relatively high amount of unexplained variance left after removal of CCA features (Fig. 5C-D, $64.5 \pm 6.7\,\%$ across individuals). While CCA does not extract features which maximize

variance in a dataset, only seeking features which maximize covariance between pitch torque and evoked DLM timing, the large amount of pitch torque signal unexplained by evoked DLM timing leaves an interesting implication. Despite the DLM being the largest muscle in *Manduca sexta*, large changes to DLM timing did not lead to large changes in tethered flight dynamics. Stated differently, the timing of one power muscle alone doesn't produce a turn.

Our results put a precise understanding on where, between the two extremes of functionally overlapping and functionally separated, the hawkmoth flight power musculature falls. By using causal electrical stimulation in concert with dual dimensionality reduction, we directly measured the degree to which a specific behavioral output, pitch torque, is driven by the control potential of a single pair of muscles, the DLMs. The DLMs do exert a measurable control potential on pitch torque sufficient to produce pitch turns (Fig. 4D, Fig. 6B), and have a consistent within-wingstroke signature on pitch torque (Fig. 4, Fig. 5). But the features of pitch torque associated with the timing of the DLMs fail to explain most of the variation in pitch torque (Fig. 5D) and poorly describe quantities on the timescale of the entire wingstroke, such as pitch angular impulse (Fig. 6A) or any wingstroke-averaged torques (Fig. S3). These results show that in controlling body pitch, at least some subset of the flight musculature *must* be coordinated to produce a pitch turn. Even if all the flight muscles have fully separate and non-overlapping kinematic functions, to produce the results observed these muscles must have some functional overlap in pitch torque.

This fits well with prior results in hawkmoths and other flying insects, where measurable functional overlap and interactions between muscles means that adequate descriptions of behavior require the activity of many coordinated muscles. In flies the 1st and 2nd basalar muscles are frequently correlated to stroke amplitude (Balint and Dickinson, 2001; Heide and Götz, 1996; Lehmann and Götz, 1996; Lindsay et al., 2017; Whitehead et al., 2015; 2022). But even these two muscles are known to have interacting kinematic effects (Dickinson and Tu, 1997; Tu and Dickinson, 1994; 1996), and the activity of at least 8 of 12 steering muscles is required to describe any more than 30 % of the variance of just wing stroke amplitude (Lindsay et al., 2017). In hawkmoths, activity from at least 4 or more muscles is needed to decode just the type of turn being performed with more than 90% accuracy (Putney et al., 2021). Similarly, redundant global information in spike timing has been observed across the entire flight motor program (Putney et al., 2019), suggesting functional coordination such that individual muscles are controlled in the context of the rest of the motor program.

Our results also provide a causal test of the temporal precision that has been estimated from information theoretic analysis of the hawkmoth flight motor program (Putney et al., 2019; 2023b). Moths were not tuned or directly cued to any particular maneuver other than wing flapping, and thus changes to DLM timing were applied across a distribution of locomotor coordination states. Precise changes in DLM timing did lead to precise changes in the CCA feature space (Fig. 6B), but these small changes were typically only a portion of the variation in the rest of the motor program (Fig. 6A). Thus, precision is relative to coordination. While the spike timing of a muscle may describe the yaw torque of a hawkmoth to

a sub-millisecond scale (Putney et al., 2023b), this is only in the context of the rest of the motor program also aiming to produce that yaw torque. When muscles functionally overlap to control an outcome like pitch or yaw torque, then the specific timing of one muscle is context-dependent, with an impact which can be cancelled out by other muscles.

Overall, then, our results underline the importance of coordination in flight musculature to produce controlled flight. While kinematic or behavioral outcomes can be causally attributed to the spike timing of individual muscles, there is enough functional overlap between muscles in the flight motor program to make the effects of muscle spike timing context-dependent. Even the largest and most powerful muscles in a hawkmoth have only so much explanatory power when manipulated outside of the coordinated activity of all other muscles.

Acknowledgements

We would like to acknowledge the other members of the agile systems lab for their discussions, support, and feedback.

Competing Interests

No competing interests declared.

Contribution

LW conceptualized, performed, and analyzed muscle stimulation experiments. JP conceptualized, performed, and analyzed high-amplitude optomotor turns experiments. SS guided project concept and facilitated experiments and analysis. LP and SS wrote and edited draft.

Funding

Air Force Office of Scientific Research grants FA9550-19-1-0396 and FA955022-1-0315, Klingenstein-Simons Fellowship Award in Neuroscience, and Dunn Family endowment to S.S.

Data availability

High-amplitude optomotor induced turns data is available on Dryad (Putney et al., 2023a), as is electrical stimulation experiment data (Wood et al., 2024). Code for optomotor turns analysis is available upon request, code for electrical stimulation experiment analysis is available on Github under https://github.com/LeoJW/stimPitchAnalysis.

Supplementary

Supplementary figures and text included.

References

Suyash Agrawal, Bret W Tobalske, Zafar Anwar, Haoxiang Luo, Tyson L Hedrick, and Bo Cheng. Musculoskeletal wing-actuation model of hummingbirds predicts diverse effects of primary flight muscles in hovering flight. *Proceedings of the Royal Society B*, 289(1988):20222076, 2022.

Noriyasu Ando and Ryohei Kanzaki. Changing motor patterns of the 3rd axillary muscle activities associated with longitudinal control in freely flying hawkmoths. *Zoological science*, 21(2):123–130, 2004.

Noriyasu Ando and Ryohei Kanzaki. Flexibility and control of thorax deformation during hawkmoth flight. *Biology letters*, 12(1):20150733, 2016.

Claire N Balint and Michael H Dickinson. The correlation between wing kinematics and steering muscle activity in the blowfly calliphora vicina. *Journal of experimental biology*, 204(24):4213–4226, 2001.

Claire N Balint and Michael H Dickinson. Neuromuscular control of aerodynamic forces and moments in the blowfly, calliphora vicina. *Journal of experimental biology*, 207(22):3813–3838, 2004.

Bo Cheng, Xinyan Deng, and Tyson L Hedrick. The mechanics and control of pitching manoeuvres in a freely flying hawkmoth (manduca sexta). *Journal of Experimental Biology*, 214(24):4092–4106, 2011.

Michael H Dickinson. Haltere–mediated equilibrium reflexes of the fruit fly, drosophila melanogaster. *Philosophical Transactions of the Royal Society of London. Series B: Biological Sciences*, 354(1385):903–916, 1999.

Michael H Dickinson and Michael S Tu. The function of dipteran flight muscle. *Comparative Biochemistry and Physiology Part A: Physiology*, 116(3):223– 238, 1997.

John L Eaton et al. *Lepidopteran anatomy.* John Wiley & Sons Limited, 1988.

María José Fernández, Dwight Springthorpe, and Tyson L Hedrick. Neuromuscular and biomechanical compensation for wing asymmetry in insect hovering flight. *Journal of Experimental Biology*, pages 3631–3638, 2012.

Steven N Fry, Rosalyn Sayaman, and Michael H Dickinson. The aerodynamics of hovering flight in drosophila. *Journal of Experimental Biology*, 208(12): 2303–2318, 2005.

Mark A Frye. Effects of stretch receptor ablation on the optomotor control of lift in the hawkmoth manduca sexta. *Journal of Experimental Biology*, 204 (21):3683–3691, 2001.

Shefa Gordon and Michael H Dickinson. Role of calcium in the regulation of mechanical power in insect flight. *Proceedings of the National Academy of Sciences*, 103(11):4311–4315, 2006.

Anders Hedenström. How insect flight steering muscles work. *PLoS biology*, 12 (3):e1001822, 2014.

Tyson L Hedrick and Thomas Lewis Daniel. Flight control in the hawkmoth manduca sexta: the inverse problem of hovering. *Journal of Experimental Biology*, 209(16):3114–3130, 2006.

Tyson L Hedrick, Jorge Martínez-Blat, and Mariah J Goodman. Flight motor modulation with speed in the hawkmoth manduca sexta. *Journal of insect physiology*, 96:115–121, 2017.

Gerhard Heide and Karl G Götz. Optomotor control of course and altitude in drosophila melanogaster is correlated with distinct activities of at least three pairs of flight steering muscles. *The Journal of experimental biology*, 199(8): 1711–1726, 1996.

Daniel N Hill, John C Curtis, Jeffrey D Moore, and David Kleinfeld. Primary motor cortex reports efferent control of vibrissa motion on multiple timescales. *Neuron*, 72(2):344–356, 2011.

Armin J Hinterwirth and Thomas L Daniel. Antennae in the hawkmoth manduca sexta (lepidoptera, sphingidae) mediate abdominal flexion in response to mechanical stimuli. *Journal of Comparative Physiology A*, 196(12):947–956, 2010.

FSJ Hollick. The flight of the dipterous fly muscina stabulans fallén. *Philosophical Transactions of the Royal Society of London. Series B, Biological Sciences*, 230(572):357–390, 1940.

Mark Jankauski, Tom Lewis Daniel, and IY Shen. Asymmetries in wing inertial and aerodynamic torques contribute to steering in flying insects. *Bioinspiration & biomimetics*, 12(4):046001, 2017.

AE Kammer. Flying. In Gerald A Kerkut, Lawrence I Gilbert, et al., editors, *Comprehensive insect physiology, biochemistry and pharmacology*, pages 491– 552. Pergamon Oxford, 1985.

Ann E Kammer. The motor output during turning flight in a hawkmoth, manduca sexta. *Journal of Insect Physiology*, 17(6):1073–1086, 1971.

Joong-Kwan Kim and Jae-Hung Han. A multibody approach for 6-dof flight dynamics and stability analysis of the hawkmoth manduca sexta. *Bioinspiration & biomimetics*, 9(1):016011, 2014.

Joong-Kwan Kim, Jong-Seob Han, Jun-Seong Lee, and Jae-Hung Han. Hovering and forward flight of the hawkmoth manduca sexta: trim search and 6-dof dynamic stability characterization. *Bioinspiration & biomimetics*, 10 (5):056012, 2015.

Jason J Kutch and Francisco J Valero-Cuevas. Muscle redundancy does not imply robustness to muscle dysfunction. *Journal of biomechanics*, 44(7):1264– 1270, 2011.

Viet Le, Benjamin Cellini, Rudolf Schilder, and Jean-Michel Mongeau. Hawkmoths regulate flight torques with their abdomen for yaw control. *Journal of Experimental Biology*, 226(9):jeb245063, 2023.

FO Lehmann and KG Götz. Activation phase ensures kinematic efficacy in flight-steering muscles of drosophila melanogaster. *Journal of comparative physiology A*, 179(3):311–322, 1996.

Fritz-Olaf Lehmann, Dimitri A Skandalis, and Ruben Berthé. Calcium signalling indicates bilateral power balancing in the drosophila flight muscle during manoeuvring flight. *Journal of The Royal Society Interface*, 10(82):20121050, 2013.

Theodore Lindsay, Anne Sustar, and Michael Dickinson. The function and organization of the motor system controlling flight maneuvers in flies. *Current Biology*, 27(3):345–358, 2017.

Johan M Melis, Igor Siwanowicz, and Michael H Dickinson. Machine learning reveals the control mechanics of an insect wing hinge. *Nature*, pages 1–9, 2024.

Gerbera Nalbach and Roland Hengstenberg. The halteres of the blowfly calliphora: Ii. three-dimensional organization of compensatory reactions to real and simulated rotations. *Journal of Comparative Physiology A*, 175:695–708, 1994.

F. Pedregosa, G. Varoquaux, A. Gramfort, V. Michel, B. Thirion, O. Grisel, M. Blondel, P. Prettenhofer, R. Weiss, V. Dubourg, et al. Scikit-learn: Machine learning in Python. *Journal of Machine Learning Research*, 12: 2825–2830, 2011.

Jose Pinheiro, Douglas Bates, Saikat DebRoy, Deepayan Sarkar, and R Core Team. *nlme: Linear and Nonlinear Mixed Effects Models*, 2020. URL https: //CRAN.R-project.org/package=nlme. R package version 3.1-147.

Joy Putney, Rachel Conn, and Simon Sponberg. Precise timing is ubiquitous, consistent, and coordinated across a comprehensive, spike-resolved flight motor program. *Proceedings of the National Academy of Sciences*, 116(52):26951– 26960, 2019.

Joy Putney, Marko Angjelichinoski, Robert Ravier, Silvia Ferrari, Vahid Tarokh, and Simon Sponberg. Consistent coordination patterns provide near perfect behavior decoding in a comprehensive motor program for insect flight. *bioRxiv*, 2021.

Joy Putney, Marko Anjelichinoski, Robert Ravier, Silvia Ferrari, Vaheed Tarokh, and Simon Sponberg. Consistent coordination patterns provide near perfect behavior decoding in a comprehensive motor program for insect flight. *Dryad, Dataset*, https://doi.org/10.5061/dryad.msbcc2g0r, 2023a.

Joy Putney, Tobias Niebur, Leo Wood, Rachel Conn, and Simon Sponberg. An information theoretic method to resolve millisecond-scale spike timing precision in a comprehensive motor program. *PLOS Computational Biology*, 19(6):e1011170, 2023b.

R Core Team. *R: A Language and Environment for Statistical Computing*. R Foundation for Statistical Computing, Vienna, Austria, 2020. URL https: //www.R-project.org/.

Shai Revzen and John M Guckenheimer. Estimating the phase of synchronized oscillators. *Physical Review E*, 78(5):051907, 2008.

Mary B Rheuben. Quantitative comparison of the structural features of slow and fast neuromuscular junctions in manduca. *Journal of Neuroscience*, 5(7): 1704–1716, 1985.

Mary B Rheuben and AE Kammer. Structure and innervation of the third axillary muscle of manduca relative to its role in turning flight. *Journal of Experimental Biology*, 131(1):373–402, 1987.

Leif Ristroph, Gunnar Ristroph, Svetlana Morozova, Attila J Bergou, Song Chang, John Guckenheimer, Z Jane Wang, and Itai Cohen. Active and passive stabilization of body pitch in insect flight. *Journal of The Royal Society Interface*, 10(85):20130237, 2013.

Sufia Sadaf, O Venkateswara Reddy, Sanjay P Sane, and Gaiti Hasan. Neural control of wing coordination in flies. *Current Biology*, 25(1):80–86, 2015.

Hirotaka Sato and Michel M Maharbiz. Recent developments in the remote radio control of insect flight. *Frontiers in neuroscience*, 4:199, 2010.

Hirotaka Sato, Tat Thang Vo Doan, Svetoslav Kolev, Ngoc Anh Huynh, Chao Zhang, Travis L Massey, Joshua Van Kleef, Kazuo Ikeda, Pieter Abbeel, and Michel M Maharbiz. Deciphering the role of a coleopteran steering muscle via free flight stimulation. *Current Biology*, 25(6):798–803, 2015.

Samuel J Sober, Simon Sponberg, Ilya Nemenman, and Lena H Ting. Millisecond spike timing codes for motor control. *Trends in neurosciences*, 41(10): 644–648, 2018.

S Sponberg and TL Daniel. Abdicating power for control: a precision timing strategy to modulate function of flight power muscles. *Proceedings of the Royal Society B: Biological Sciences*, 279(1744):3958–3966, 2012.

Simon Sponberg, Andrew J Spence, Chris H Mullens, and Robert J Full. A single muscle's multifunctional control potential of body dynamics for postural control and running. *Philosophical Transactions of the Royal Society B: Biological Sciences*, 366(1570):1592–1605, 2011.

Simon Sponberg, Thomas L Daniel, and Adrienne L Fairhall. Dual dimensionality reduction reveals independent encoding of motor features in a muscle synergy for insect flight control. *PLoS computational biology*, 11(4):e1004168, 2015a.

Simon Sponberg, Jonathan P Dyhr, Robert W Hall, and Thomas L Daniel. Luminance-dependent visual processing enables moth flight in low light. *Science*, 348(6240):1245–1248, 2015b.

Dwight Springthorpe, María José Fernández, and Tyson L Hedrick. Neuromuscular control of free-flight yaw turns in the hawkmoth manduca sexta. *Journal of Experimental Biology*, 215(10):1766–1774, 2012.

AL Stöckl, David O'Carroll, and EJ Warrant. Higher-order neural processing tunes motion neurons to visual ecology in three species of hawkmoths. *Proceedings of the Royal Society B: Biological Sciences*, 284(1857):20170880, 2017.

Haithem E Taha, Mohammadali Kiani, Tyson L Hedrick, and Jeremy SM Greeter. Vibrational control: A hidden stabilization mechanism in insect flight. *Science Robotics*, 5(46):eabb1502–eabb1502, 2020.

GK Taylor and ALR Thomas. Animal flight dynamics ii. longitudinal stability in flapping flight. *Journal of theoretical biology*, 214(3):351–370, 2002.

Graham K Taylor. Mechanics and aerodynamics of insect flight control. *Biological Reviews*, 76(4):449–471, 2001.

Lena H Ting. Dimensional reduction in sensorimotor systems: a framework for understanding muscle coordination of posture. *Progress in brain research*, 165:299–321, 2007.

Wei Mong Tsang, Alice L Stone, Zane N Aldworth, John G Hildebrand, Tom L Daniel, Akintunde Ibitayo Akinwande, and Joel Voldman. Flexible split-ring electrode for insect flight biasing using multisite neural stimulation. *IEEE Transactions on Biomedical Engineering*, 57(7):1757–1764, 2010.

M Tu and M Dickinson. Modulation of negative work output from a steering muscle of the blowfly calliphora vicina. *The Journal of experimental biology*, 192(1):207–224, 1994.

Michael S Tu and Thomas L Daniel. Submaximal power output from the dorsolongitudinal flight muscles of the hawkmoth manduca sexta. *Journal of Experimental Biology*, 207(26):4651–4662, 2004.

MS Tu and MH Dickinson. The control of wing kinematics by two steering muscles of the blowfly (calliphora vicina). *Journal of Comparative Physiology A*, 178(6):813–830, 1996.

PNR Usherwood. The nature of 'slow'and 'fast'contractions in the coxal muscles of the cockroach. *Journal of Insect Physiology*, 8(1):31–52, 1962.

Francisco J Valero-Cuevas. A mathematical approach to the mechanical capabilities of limbs and fingers. *Progress in Motor Control: a Multidisciplinary Perspective*, pages 619–633, 2009.

Rick J Vazquez. Functional anatomy of the pigeon hand (columba livia): a muscle stimulation study. *Journal of morphology*, 226(1):33–45, 1995.

Hao Wang, Noriyasu Ando, and Ryohei Kanzaki. Active control of free flight manoeuvres in a hawkmoth, agrius convolvuli. *Journal of Experimental Biology*, 211(3):423–432, 2008.

Jacob A Wegelin. A survey of partial least squares (pls) methods, with emphasis on the two-block case. 2000.

Samuel C Whitehead, Tsevi Beatus, Luca Canale, and Itai Cohen. Pitch perfect: how fruit flies control their body pitch angle. *Journal of Experimental Biology*, 218(21):3508–3519, 2015.

Samuel C Whitehead, Sofia Leone, Theodore Lindsay, Matthew R Meiselman, Noah J Cowan, Michael H Dickinson, Nilay Yapici, David L Stern, Troy Shirangi, and Itai Cohen. Neuromuscular embodiment of feedback control elements in drosophila flight. *Science Advances*, 8(50):eabo7461, 2022.

Alexander P Willmott and Charles P Ellington. The mechanics of flight in the hawkmoth manduca sexta. i. kinematics of hovering and forward flight. *Journal of experimental Biology*, 200(21):2705–2722, 1997.

Shane P Windsor, Richard J Bomphrey, and Graham K Taylor. Vision-based flight control in the hawkmoth hyles lineata. *Journal of The Royal Society Interface*, 11(91):20130921, 2014.

Leo Wood, Joy Putney, and Simon Sponberg. Flight power muscles have a coordinated, causal role in controlling hawkmoth pitch turns. *Dryad, Dataset*, https://doi.org/10.5061/dryad.76hdr7t4f, 2024.

Johannes M Zanker. On the mechanism of speed and altitude control in drosophila melanogaster. *Physiological entomology*, 13(3):351–361, 1988.

Figures

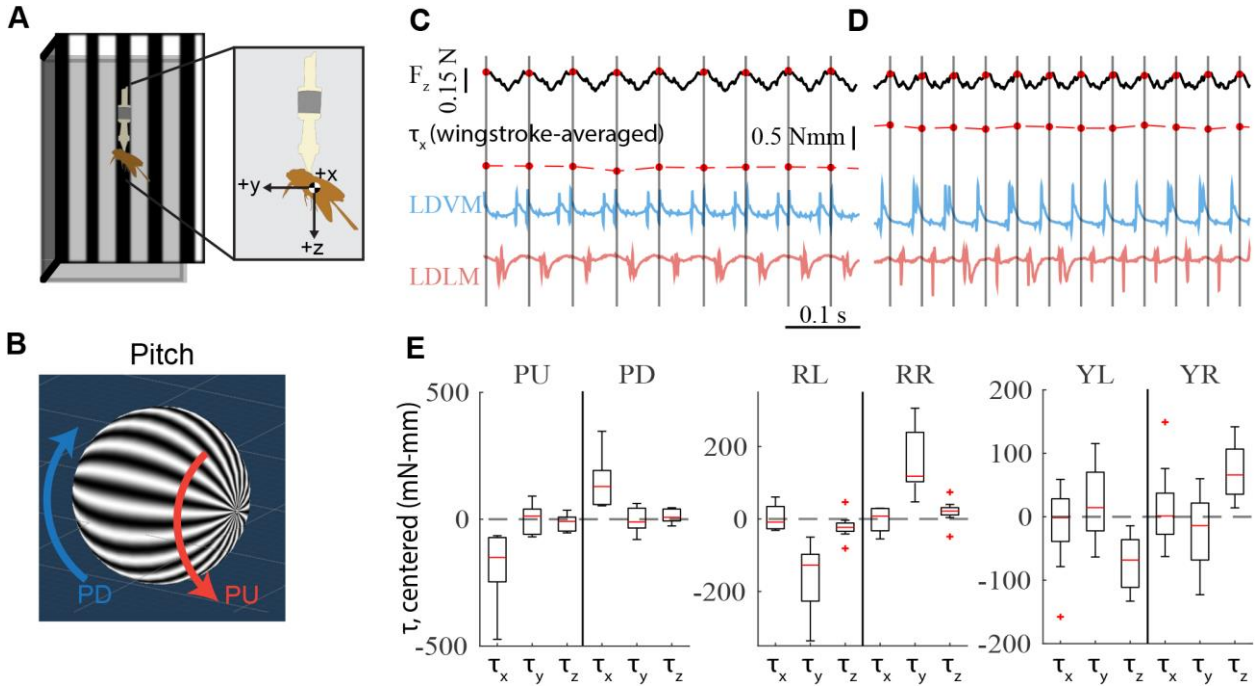

Fig. 1. Constant high-amplitude optomotor turns produce separated body torque responses.

Tethered moths were shown three pairs of visual stimuli to elicit high-amplitude turns about the three flight axes – pitch, roll and yaw. (**A**) Schematic of the visual stimulus arena formed by three computer monitors, with the moth tethered in the center. Inset depicts coordinate frame used throughout. (**B**) Example of wide-field stimuli in pitch direction. Widefield sinusoidal gratings on a projected 3D sphere, with spheres rotated with a constant drift velocity produce two different stimulus conditions for each axis of rotation. (**C-D**) Simultaneous raw EMG recordings of the left side power muscles with motor output for 0.5 s in the pitch up (C) and pitch down (D) conditions. Wingstrokes were segmented using the Hilbert transform of F_z force. Wingstroke averaged pitch torque (τ_x) demonstrates different behavior in response to the visual stimulus conditions. (**E**) Centered mean wingstroke averaged pitch (τ_x), roll (τ_y), and yaw (τ_z) torques for each individual moth ($N = 9$) in six conditions.

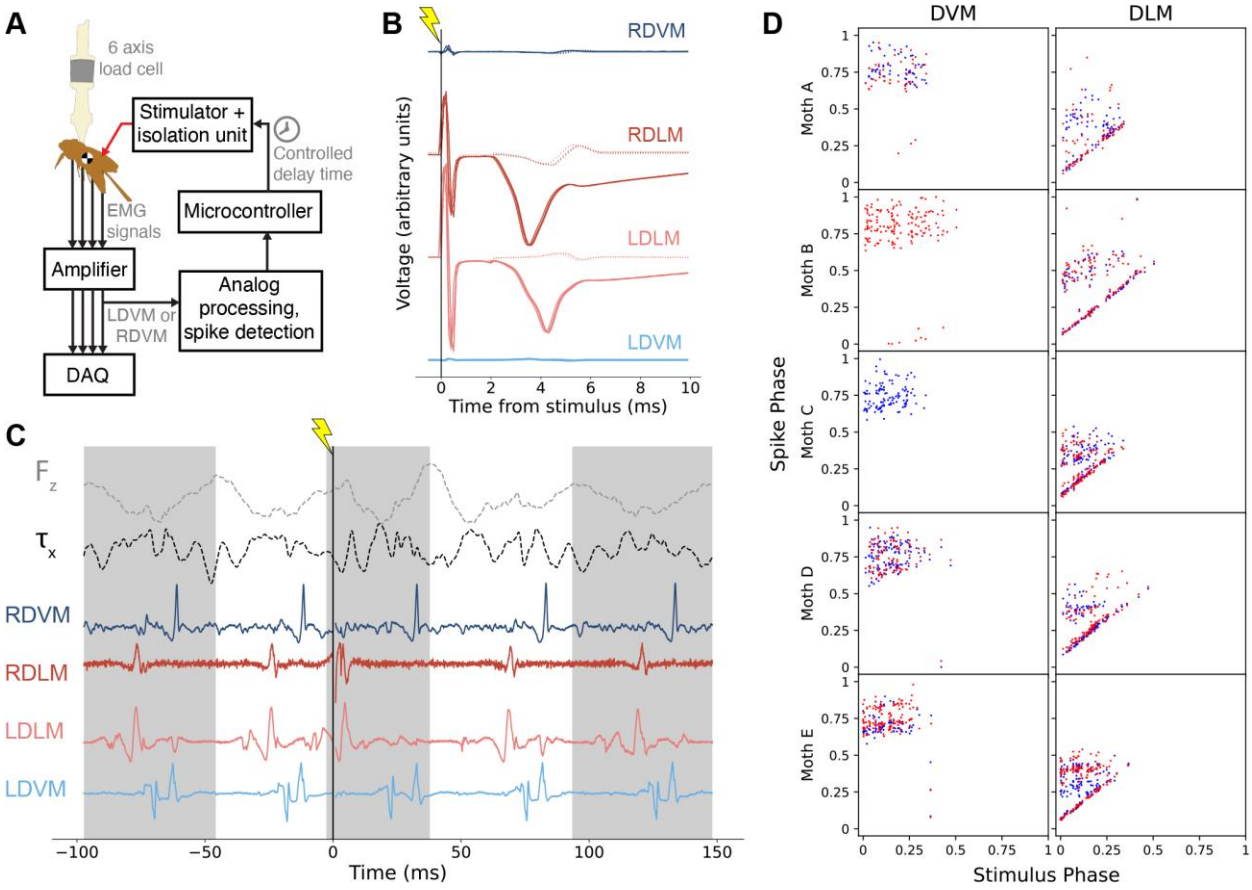

Fig. 2. Electrical stimulation allows controlled change of DLM timing, leading to changes in body pitch torque.

(**A**) Diagram of stimulation experiment signal flow. Analog spike detection is run on a DVM signal post-amplification, enabling a microcontroller to trigger a stimulator with specific timings relative to observed DVM spikes (see (Sponberg and Daniel, 2012) for a similar experiment). (**B**) Voltage recordings, aligned at time of stimulus, from all four power muscles in a quiescent moth while stimulation is applied, illustrating efficacy of electrical stimulation. Lighter dotted traces are 0.03 mA current of stimulation, darker solid traces are 0.05 mA current. (**C**) Example trace of EMG and vertical force and pitching torque data during stimulation. Stimulation is applied at time $t = 0$ (denoted by vertical line with lightning symbol) and produces a phase advance in RDLM and LDLM spikes. Alternating shaded regions indicate wingstrokes found via negative-to-positive zero crossings of the Hilbert transform of F_z (light grey dashed line). (**D**) Phase of all

spikes in stimulation wingstroke plotted against the phase at which stimulation was applied for that wingstroke on the x axis. Red points indicate right muscle, blue points left muscle. If stimulation is inducing spikes in the DLM, then spikes along an identity line should be observed only in the right DLM column. Note that mean natural DLM phase of this dataset is at 32.7% of the wingstroke.

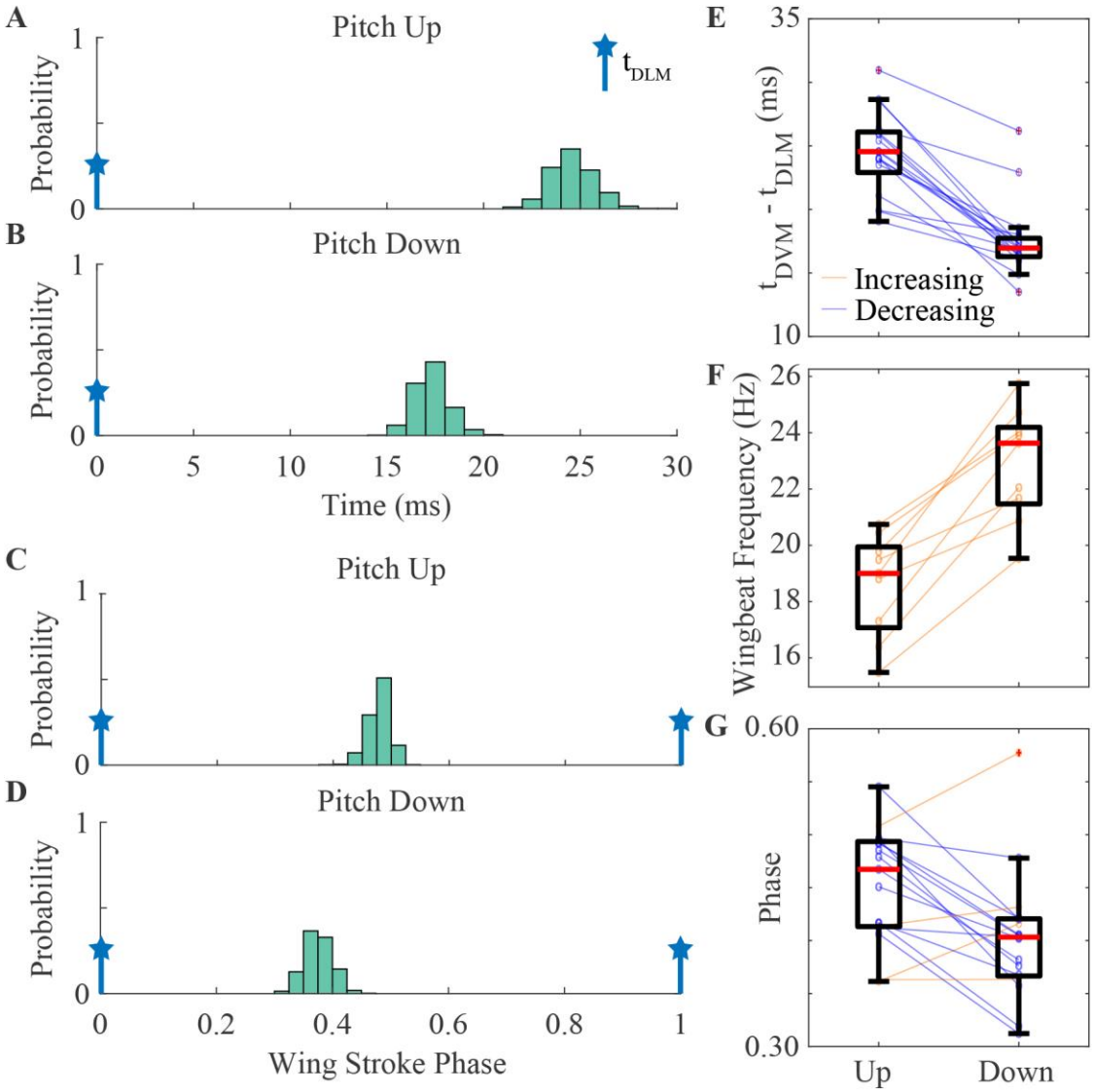

Fig. 3. Timing between the DVM and DLM muscles increases when moths pitch up.

(**A-B**) Normalized histograms from an example moth of the first DVM spike timing in each wing stroke (t_{DVM}) with respect to the DLM timing ($t_{DLM} = 0$) for the pitch up and pitch down conditions. (**C-D**) Normalized histograms from the same example moth of the phase of the first DVM spike in each wing stroke with respect to the DLM timing. (**E**) Absolute timing difference between t_{DVM} and t_{DLM} for 17 same-side DLM-DVM pairs ($N = 9$ moths for 19 same-side pairs, with one failed DVM recording eliminating a pair). Means are statistically different, $p < 10^{-6}$ for paired t-test. (**F**) Wingbeat frequency for all

9 moths for the pitch up and pitch down conditions (means statistically different, $p < 10^{-3}$ for paired t-test). (**G**) Phase of the first DVM spike in each wing stroke with respect to the DLM timing for 17 same-side DLM-DVM pairs (means statistically different, $p = 0.003$ for paired t-test). Boxplots report the mean across individuals (red line), the 25th and 75th percentiles (box region), and the total range (whiskers) excluding outliers (red crosses).

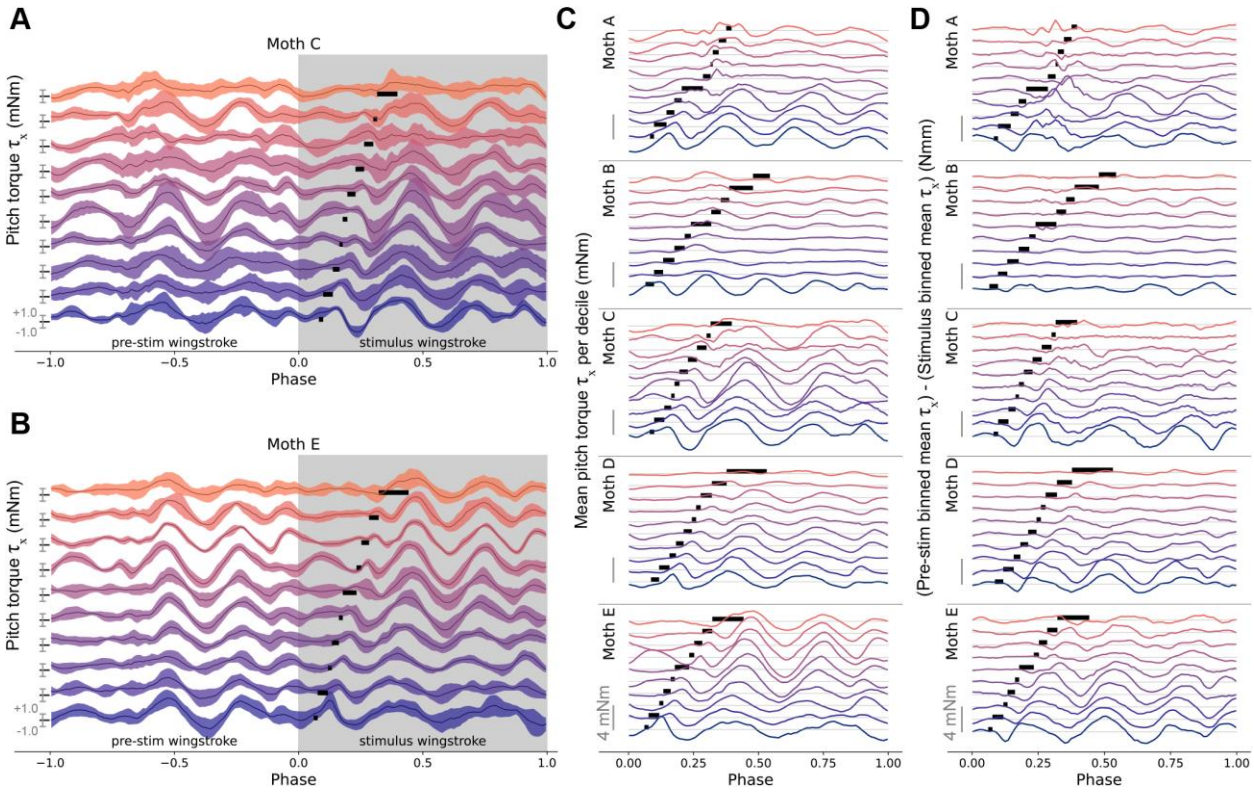

Fig. 4. Qualitative features of stimulation visible in mean pitch torque waveforms binned by decile of stimulation phase.

(**A,B**) Mean ± 1 standard deviation (S.D.) of time-varying pitch torque in the wingstrokes before, during, and after stimulation for two example individuals, binned by decile of stimulation phase. Each binned mean ± S.D. trace contains the same number of pitch torque traces. Bars in stimulus wingstroke indicate the minimum to maximum range of phases during which stimulus was applied for each binned group. Axes on left of each trace indicate where pitch torque (in mNm) is zero, +1, and −1 for each group. (**C**) Plots following (A) and (B) for all individuals, but showing only mean pitch torque for only the stimulation wingstroke. Light grey line indicates zero mNm for each binned decile. (**D**) Difference in mean pitch torque during stimulated wingstroke compared to pre-stimulation wingstroke. At each phase the difference $\boldsymbol{\tau_{x,pre} - \tau_{x,stim}}$ is taken, so this plot indicates the deviation from undisturbed, pre-stimulation pitch torque profile. Scale bars indicate 4 mNm for each individual, light grey line indicates zero mNm for each decile.

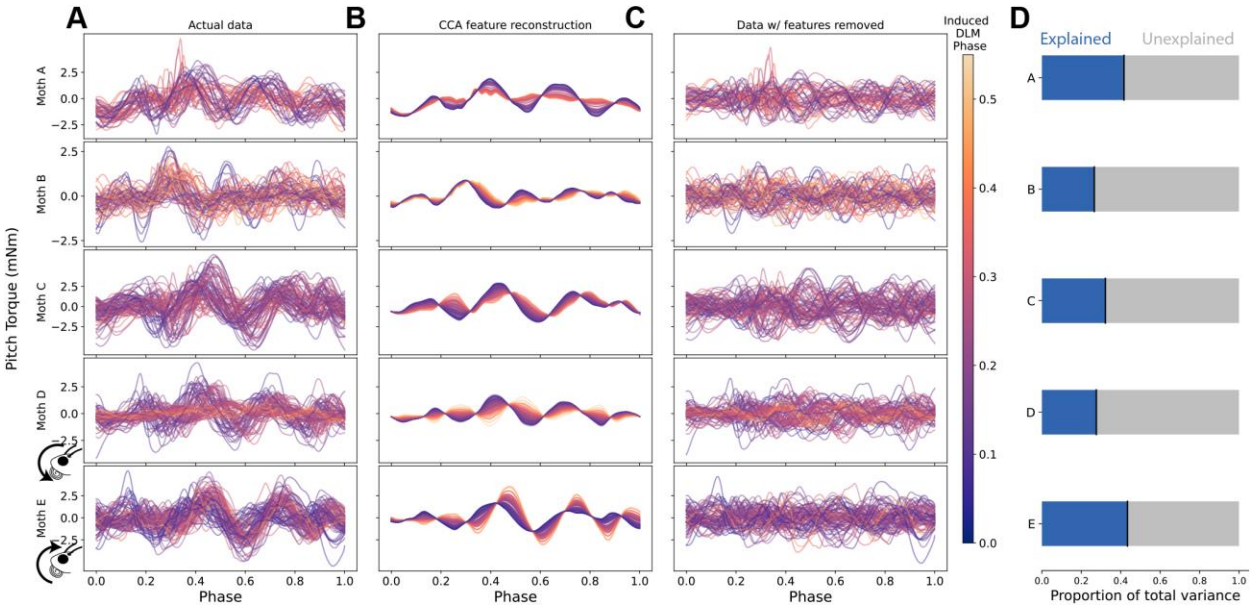

Fig. 5. Features of pitch torque which covary with evoked DLM timing show consistent phase shift in pitch torque. (**A**) Actual data of pitch torque in stimulation wingstroke, colored by evoked DLM phase on the same scale as (A-D). (**B**) CCA feature reconstructions of pitch torque in stimulation wingstroke, colored by evoked DLM phase. Reconstructions generated using Eq. (1) followed by removal of z-scoring. (**C**) Raw data with CCA feature reconstructions subtracted, leaving only variance in pitch torque signal unexplained by CCA features. (**D**) Proportion of total variance explained by CCA feature reconstructions (blue, left) vs. unexplained (grey, right).

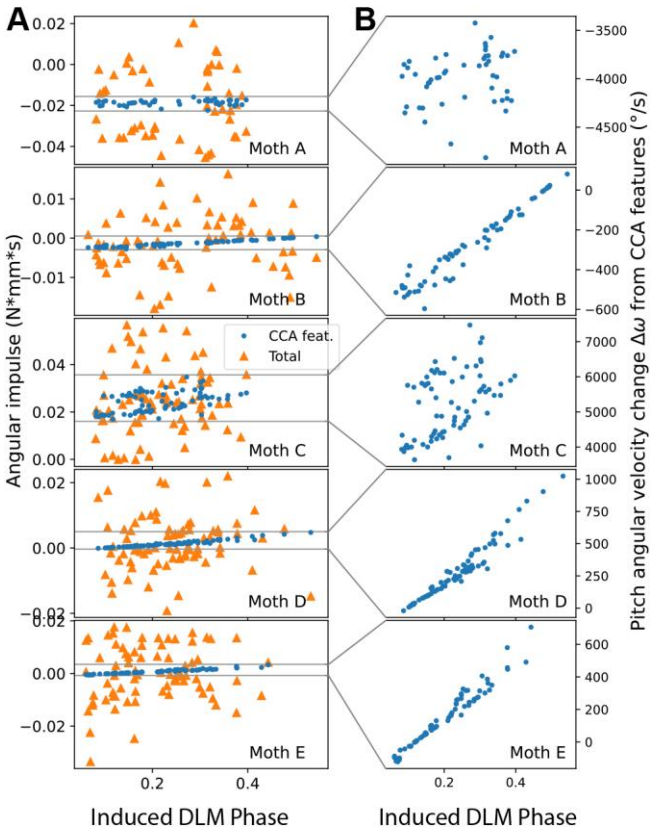

Fig. 6. CCA features produce mechanically relevant levels of angular impulse in pitch. (**A**) Overall angular impulse from pitch torque (orange, triangles, Fig. 5A) and angular impulse from *just* CCA feature reconstructions of pitch torque associated with DLM phase (blue, circles, Fig. 5B) for each individual moth. (**B**) Pitch angular velocity change due to angular impulse from CCA feature reconstructions, in degrees per second.

Supplementary Information

1 Nonlinear Kernel CCA

The CCA analysis of the main text is inherently linear in nature, constituting a reprojection of the pitch torque waveforms guided to maximize cross-covariance with induced DLM phase. It is possible that some of the key features of the pitch torque which varied with DLM phase might be inherently nonlinear. So, it is relevant to assess to what degree a nonlinear dual-dimensionality reduction method could perform better, and whether a nonlinear method extracts fundamentally different features from the pitch torque data. To that end, we performed kernel CCA (KCCA), a variant of the traditional CCA with an nonlinear kernel transform of the component variables. See (Akaho, 2006) and (Hardoon et al., 2004) for review, examples, and deeper coverage of kernel CCA. In brief, in KCCA both sets of data $\boldsymbol{\tau}$ and $\boldsymbol{Y}$ are projected into a high-dimensional reproducing kernel Hilbert space using a kernel function $\phi(X)$ and traditional CCA is performed on the kernel space representations of the data $\phi(\boldsymbol{\tau})$ and $\phi(\boldsymbol{Y})$. By performing the normally linear CCA in this high-dimensional space, it can capture transformations which would be nonlinear in the original basis, with minimal additional computational complexity compared to normal CCA.

KCCA does require a choice of a positive definite kernel function $\phi(X)$, and results can be sensitive to both the choice of this function and any constant parameters defining the function. We opted to use the radial basis function, also known a the Gaussian kernel, as our kernel, defined by

$$\phi(x, y) = e^{-\gamma||x-y||^2} \tag{1}$$

as it is commonly used, implicitly defines an infinite-dimensional Hilbert space, and requires choice of only a single parameter γ which defines the width of the radial Gaussian.

One downside of KCCA is that kernel functions are rarely invertible, so there does not always exist a well defined function $\phi^{-1}(X)$. This has the consequence of making it relatively easy to find a latent space in which two sets of variables $\boldsymbol{\tau}$ and $\boldsymbol{Y}$ are maximally correlated, but moving back from this latent space to reconstruct features in the original data space which the KCCA extracted, as we do in the main text using Eq. (1), is not directly possible.

To evaluate the features extracted by KCCA, and how much of the variance in pitch torque $\boldsymbol{\tau}$ they explain, we followed a common solution first proposed by Bakır et al (Bakır

et al., 2004) and adapted from the implementation in scikit-learn's KernelPCA class (Pedregosa et al., 2011). In this technique, rather than try to evaluate $\phi^{-1}(X)$, a function Γ is estimated which approximately satisfies $\Gamma(\phi(\boldsymbol{\tau}_i)) = \boldsymbol{\tau}_i$ for all n wingstrokes $i = 1, \ldots, n$, in our case using a kernel ridge regression.

The results of running KCCA and estimating an inverse transform to reconstruct pitch torque features is shown in Fig. S1. To ensure the KCCA explained as much variance in pitch torque as possible, the parameter $\gamma = 0.4018$ was chosen as it maximizes the mean r^2 across moths between pitch torque reconstructions and the actual pitch torque waveforms, as shown in Fig. S2. Compared to the linear CCA, this nonlinear method explained on average 7.4% more variance in pitch torque. Crucially, however, it did not extract any features of the pitch torque waveforms that differed dramatically from the features found via linear CCA. While the nonlinear method was able to extract pitch torque waveforms that did not simply rescale based on induced DLM timing, both methods extracted features consisting of 3-4 major peaks with a pronounced phase shift in the largest peak associated with later induced DLM phase. This indicates that there is an underlying relationship between induced DLM phase and pitch torque which is robust to the particular method of feature identification. while a nonlinear method may be able to explain slightly more variance, it is unlikely to extract significantly different features of pitch torque, is more complicated, and does not allow for explicit invertibility.

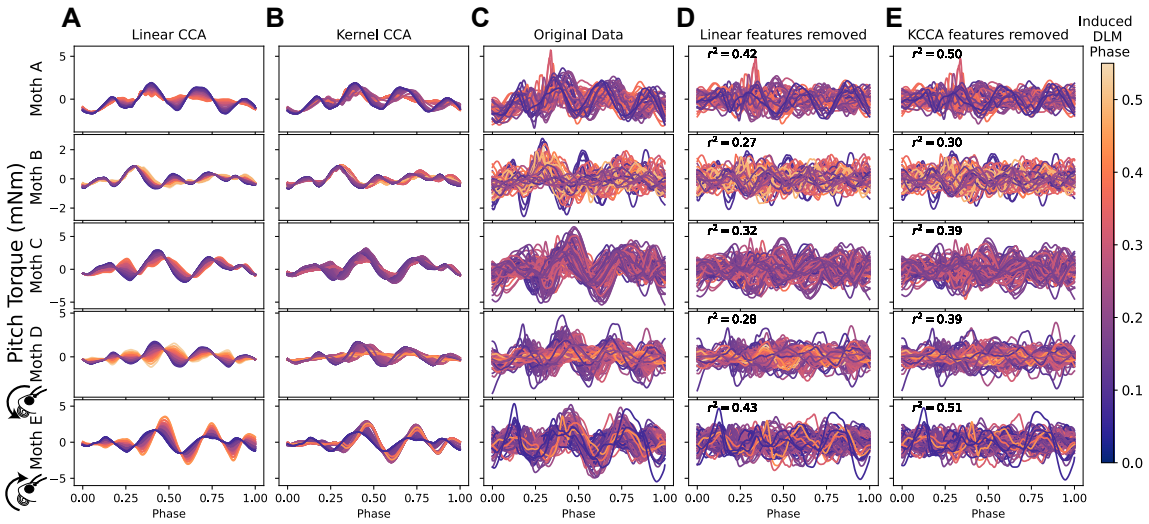

Fig. S1. Pitch torque features extracted from kernel and regular CCA. (**A**) Linear CCA feature reconstructions of pitch torque in stimulation wingstroke, colored by evoked DLM phase. (**B**) Nonlinear kernel CCA feature reconstructions, colored on the same scale as (A-E) (**C**) Actual data of pitch torque in stimulation wingstroke (**D**) Raw data with linear CCA feature reconstructions subtracted, leaving only pitch torque variance unexplained by linear CCA features. r^2 for feature reconstructions printed for each moth. (**E**) Raw data with nonlinear kernel CCA feature reconstructions subtracted. r^2 for feature reconstructions printed for each moth.

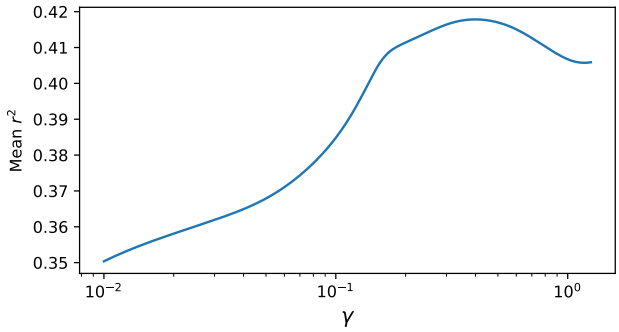

Fig. S2. Parameter search for optimal γ. KCCA is performed between induced DLM phase and pitch torque waveforms with the radial basis function kernel of Eq. (1) across varying values of γ, for all data in dataset. At each γ pitch torque reconstructions are performed and the r^2 of these reconstructions compared to the actual pitch torque data are calculated, for each moth. This line shows the mean r^2 value across all moths, with the peak value being used to select for γ in further analysis.

Table S1. Results of linear mixed-effects models. Coefficient estimate *beta* and p-value of that estimate for linear mixed-effects models run between each force or torque and induced DLM timing. Rows are bolded if the relationship is statistically significant ($p < 0.05$). Each model was of the form $F_x \sim \beta Y$ where Y is induced DLM phase, and an additional random constant effect is added to account for individual variation. All models were fit using the nlme package (Pinheiro et al., 2020) in the R language (R Core Team, 2020).

Variable	coefficient β	p-value
F_x	-0.000612	0.51
$\boldsymbol{F_y}$	**-0.00627**	**1e-4**
$\boldsymbol{F_z}$	**0.0049**	**0.045**
T_x	-0.012	0.11
T_y	-0.0119	0.89
T_z	0.02	0.62

2 Induced DLM timing and wingstroke-averaged forces and torques

In the main text, DLM timing was shown to induce a within-wingstroke change in pitch torque, yet through the results of Fig. 6 this change was implicated as relatively minor in the presence of the much greater variation in pitch torque present from other sources in the motor program. To further bolster this analysis, we investigated the degree to which wingstroke-averaged forces and torques correlate with induced DLM phase.

As shown in Fig. S3, wingstroke-averaged forces and torques have little clear relationship with induced DLM phase. To measure whether there was any significant linear relationship between induced DLM phase and any of the wingstroke-averaged forces and torques, we ran linear mixed-effects models between induced DLM phase and wingstroke-averaged values for each force and torque with moth as a random constant effect, the results of which are summarized in Table S1. Induced DLM phase was a statistically significant ($p < 0.05$) predictor of only mean F_y (forward force) and F_z (vertical force). For wingstroke-averaged pitch torque, the primary focus of this paper, there was no detectable relationship between stimulation-induced DLM phase and the resulting mean pitch torque. That said, just because there is no significant correlation with mean wingstroke torque, does not mean that DLM phase has no consistent effect. There were clear within-wingstroke changes to pitch torque due to controlled changes to DLM timing which were on their own mechanically relevant (as can be seen in Fig. 4 and Fig. 5). These changes, however, wash out behind the natural variation present in the rest of the motor program over the course of an entire wingstroke.

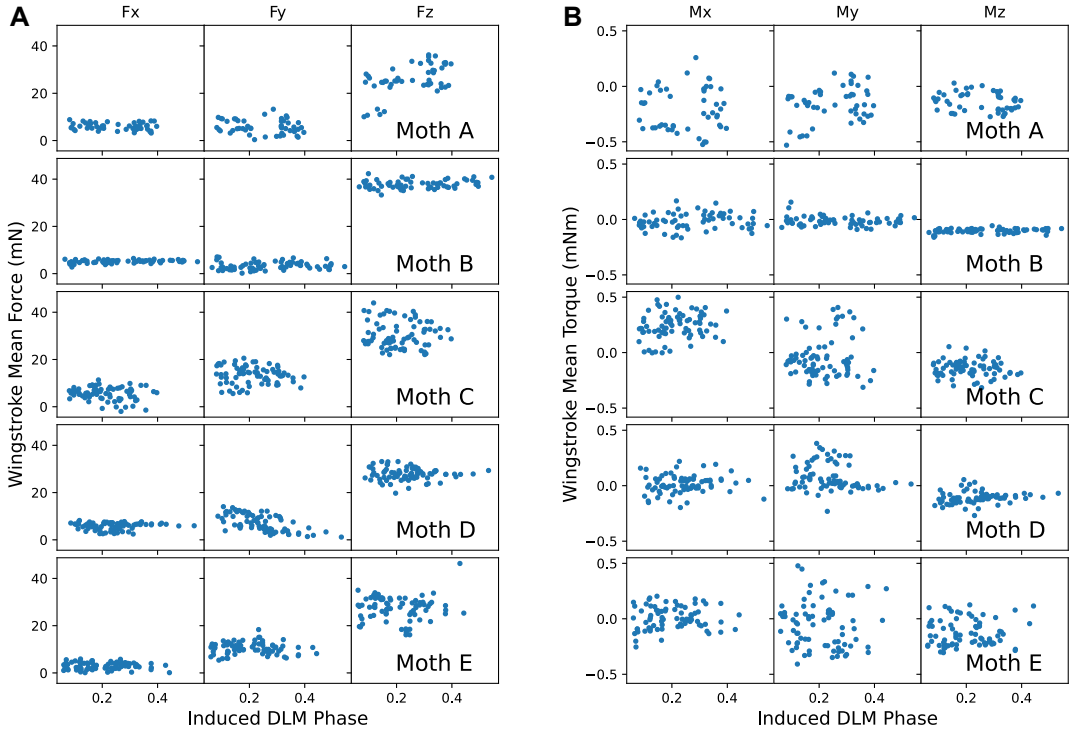

Fig. S3: **Wingstroke mean forces and torques against induced DLM phase**. (**A**) Wingstroke mean forces in X, Y, and Z directions for stimulation wingstrokes plotted against stimulation-induced DLM phase. Directions follow convention of Fig. 1 in the main text (F_y is forward, F_x is lateral, F_z is dorso-ventral). (**B**) Wingstroke mean torques in X, Y, and Z directions for stimulation wingstrokes plotted against stimulation-induced DLM phase. Directions follow convention of Fig. 1 in the main text (T_x is pitch, T_y is roll, T_z is yaw).

References

Shotaro Akaho. A kernel method for canonical correlation analysis. *arXiv preprint cs/0609071*, 2006.

Gökhan H Bakır, Jason Weston, and Bernhard Schölkopf. Learning to find pre-images. *Advances in neural information processing systems*, 16:449–456, 2004.

David R Hardoon, Sandor Szedmak, and John Shawe-Taylor. Canonical correlation analysis: An overview with application to learning methods. *Neural computation*, 16(12): 2639–2664, 2004.

F. Pedregosa, G. Varoquaux, A. Gramfort, V. Michel, B. Thirion, O. Grisel, M. Blondel, P. Prettenhofer, R. Weiss, V. Dubourg, J. Vanderplas, A. Passos, D. Cournapeau, M. Brucher, M. Perrot, and E. Duchesnay. Scikit-learn: Machine learning in Python. *Journal of Machine Learning Research*, 12:2825–2830, 2011.

Jose Pinheiro, Douglas Bates, Saikat DebRoy, Deepayan Sarkar, and R Core Team. *nlme: Linear and Nonlinear Mixed Effects Models*, 2020. URL `https://CRAN.R-project.org/package=nlme`. R package version 3.1-147.

R Core Team. *R: A Language and Environment for Statistical Computing*. R Foundation for Statistical Computing, Vienna, Austria, 2020. URL `https://www.R-project.org/`.